

High Rayleigh number variational multiscale large eddy simulations of Rayleigh-Bénard Convection

David Sondak^{a,*}, Thomas M. Smith^b, Roger P. Pawłowski^b, Sidafa Conde^c, John N. Shadid^{c,d}

^a*Institute for Applied Computational Science, Harvard University, Maxwell Dworkin, Suite G107, 33 Oxford Street, Cambridge, MA 02138*

^b*Sandia National Laboratories, Computational Science Department*

^c*Sandia National Laboratories, Computational Mathematics Department*

^d*Department of Mathematics and Statistics, University of New Mexico, MSC01 1115, Albuquerque, NM 87131, USA*

Abstract

The variational multiscale (VMS) formulation is used to develop residual-based VMS large eddy simulation (LES) models for Rayleigh-Bénard convection. The resulting model is a mixed model that incorporates the VMS model and an eddy viscosity model. The Wall-Adapting Local Eddy-viscosity (WALE) model is used as the eddy viscosity model in this work. The new LES models were implemented in the finite element code Drekar. Simulations are performed using continuous, piecewise linear finite elements. The simulations ranged from $Ra = 10^6$ to $Ra = 10^{14}$ and were conducted at $Pr = 1$ and $Pr = 7$. Two domains were considered: a two-dimensional domain of aspect ratio 2 with a fluid confined between two parallel plates and a three-dimensional cylinder of aspect ratio 1/4. The Nusselt number from the VMS results is compared against three dimensional direct numerical simulations and experiments. In all cases, the VMS results are in good agreement with existing literature.

Keywords: Rayleigh-Bénard convection, large eddy simulation, variational multiscale formulation

1. Introduction

Rayleigh-Bénard convection is the buoyancy-driven flow of a fluid confined between two parallel, horizontal plates where the bottom plate is at a higher temperature than the top plate. An initially quiescent fluid will be set into motion for a sufficiently large temperature difference between the two plates. This deceptively simple configuration provides for an exceptionally rich variety of fluid motion. Indeed, Rayleigh-Bénard convection has been used as a proxy for the phenomenon of thermal convection, which is responsible for a dizzying array of fluid phenomena from the geophysical through the astrophysical. Rayleigh-Bénard convection is also known for being one of the original flow fields studied in the field of hydrodynamic stability theory [1, 2]. In his pioneering work, Rayleigh used linear stability theory to show precisely when an initially quiescent fluid will bifurcate from the quiescent, conduction state to the first convection state [3]. The primary control parameter governing this bifurcation is now known as the Rayleigh number Ra , which is a measure of the ratio of buoyancy-driven inertial forces to viscous forces. Over the years, Rayleigh-Bénard convection has been studied well beyond the theory of fluid stability.

One major research thrust has been the focus on quantifying how the heat transport through the fluid layer depends on Ra [4, 5]. The primary diagnostic quantity in Rayleigh-Bénard convection is the dimensionless heat transport expressed as the

ratio of total heat transport to conduction heat transport and called the Nusselt number (Nu). Significant theoretical, computational, and experimental resources have been devoted to determining the relationship between Nu and Ra . A major question focuses on the exponent in the power law relationship $Nu \propto Ra^\beta$. Theoretical arguments have been used to show that $\beta \approx 1/3$ [6, 7] while other rigorous mathematical arguments have established bounds that show $\beta \leq 1/2$ [8, 9]. Classical work based on turbulence mixing length models has predicted that β transitions to $1/2$ for very large Ra with logarithmic corrections in Ra [10]. Other recent work has proposed models of Nu that are not pure power laws in Ra [11]. There has been much discussion on recent experimental results at high Ra that observe a transition to $\beta = 1/2$ [12, 13] or not at very high Ra [14, 15]. Numerical calculations have shown that $\beta \approx 0.28 - 0.3$ up to the largest Ra currently achievable [16, 17]. Very recently, two-dimensional numerical simulations up to $Ra = 10^{14}$ observed a transition to $\beta = 1/2$ [18, 19], while three-dimensional simulations up to $Ra = 10^{15}$ have not observed this transition [17]. At high Ra , it becomes prohibitively expensive to perform fully-resolved direct numerical simulations of Rayleigh-Bénard convection. Hence, there is great interest in the development of turbulence models that will permit accurate simulations at high Ra .

Instead of directly resolving all scales of motion, large eddy simulation (LES) coarse grains the fields and equations and simulates only the largest scales of motion. The price to pay is that this coarse graining procedure introduces correlations between resolved and unresolved terms that cannot be neglected and must be modeled. The goal of LES turbulence modeling is

*Corresponding author

Email address: dsondak@seas.harvard.edu (David Sondak)

to develop models that account for the effect of the unresolved scales on the resolved scales. Fluid simulations with the finite element method have been challenging due to the need to satisfy (or circumvent) the inf-sup condition, satisfy the incompressibility constraint, and stabilize spurious oscillations for highly convective flows. Stabilized finite element methods were developed to overcome these challenges [20, 21] and were eventually shown to derive from the variational multiscale (VMS) method [22]. Since its original development, the VMS method has been used to develop LES models for a variety of fluid flows [23, 24, 25, 26, 27, 28]. Recently, researchers developed a VMS-based LES model for Rayleigh-Bénard convection with application to heating systems [29]. In the current work, we propose a mixed VMS method for Rayleigh-Bénard convection at high Ra . We perform simulations up to $Ra = 10^{14}$ for two different Prandtl numbers ($Pr = 1$ and $Pr = 7$) in both two and three dimensions for rectangular and cylindrical geometries.

The remainder of the paper is organized as follows. In section 2 we provide the governing equations, the VMS formulation for Rayleigh-Bénard convection, and a description of the code used to perform the simulations. Following this, section 3 presents the results of the simulations. Section 4 summarizes the work and discusses ongoing and future work.

2. Background

2.1. Rayleigh-Bénard Convection

Rayleigh-Bénard convection is concerned with the buoyancy-driven flow of a fluid confined between two parallel, horizontal plates separated by a distance H . The two plates are maintained at constant temperatures such that the temperature difference between the top and bottom plates is $\Delta T = T_{\text{bot}} - T_{\text{top}} > 0$. Within the Oberbeck-Boussinesq approximation, density variations are assumed to be important only in the buoyancy term and these variations are taken to depend linearly on the temperature. The fluid is otherwise incompressible. The velocity field $\mathbf{u}(\mathbf{x}, t) = (u, v, w)$ evolves according to the Oberbeck-Boussinesq equations,

$$\rho_0 \left(\frac{\partial \mathbf{u}}{\partial t} + \nabla \cdot (\mathbf{u} \otimes \mathbf{u}) \right) = -\nabla P + \mu \nabla^2 \mathbf{u} + \alpha_V g (T - T_0) \hat{\mathbf{y}} \quad (1)$$

$$\nabla \cdot \mathbf{u} = 0 \quad (2)$$

where $\rho_0 = \rho(T_0)$ is the reference density evaluated at a reference temperature T_0 , $P = P(\mathbf{x}, t)$ is the kinematic pressure of the fluid, μ is the kinematic viscosity, α_V is the coefficient of volume expansion of the fluid, g is the acceleration due to gravity, and $\hat{\mathbf{y}}$ is the unit vector in the vertical direction. The temperature field $T = T(\mathbf{x}, t)$ evolves according to an advection diffusion equation,

$$\rho_0 C_p \left(\frac{\partial T}{\partial t} + \nabla \cdot (\mathbf{u} T) \right) = k \nabla^2 T \quad (3)$$

where C_p and k are the specific heat and thermal conductivity of the fluid, respectively. The velocity field uses no-slip boundary conditions on all solid surfaces. The temperature is

held at a uniform constant temperature on the top and bottom surfaces such that the bottom surface is hotter than the top surface. In the present work, we consider two different geometries and therefore the boundary conditions on the “sides” are specified differently depending on which geometry is being considered. In two-dimensional Rayleigh-Bénard convection between two infinite parallel planes the velocity and temperature fields have periodic boundary conditions in the x direction. In three-dimensional Rayleigh-Bénard convection in a right circular cylinder, the surface of the cylinder is insulated and the temperature field uses homogeneous Neumann boundary conditions on the side-walls of the cylinder.

The two classical non-dimensional parameters emerging from the system in (1)- (3) are the Rayleigh and Prandtl numbers. The Prandtl number is a fluid property and is given by,

$$Pr = \frac{\nu}{\kappa} \quad (4)$$

where $\nu = \mu/\rho_0$ and $\kappa = k/(\rho_0 C_p)$. The Rayleigh number is,

$$Ra = \frac{g \alpha_V \Delta T H^3}{\nu \kappa} \quad (5)$$

and is interpreted as a measure of the strength of buoyancy-driven inertial forces. In the conduction state, the heat transport is $\mathcal{H}_{\text{cond}} = \kappa \Delta T / H$, independent of Ra and Pr . After convection sets in, the heat transport is quantified by the Nusselt number Nu as the ratio of total heat transfer to conduction heat transfer. The Nusselt number is,

$$Nu = - \frac{H}{\Delta T} \overline{\left. \frac{dT}{dy} \right|_{y_{\text{wall}}}} \quad (6)$$

where $\overline{\cdot}$ represents an average over the plane orthogonal to the wall-normal coordinate. In statistically steady state, after integrating across the width of the fluid layer, the Nusselt number can be written as,

$$Nu = 1 + \frac{\langle vT \rangle}{\mathcal{H}_{\text{cond}}} \quad (7)$$

where $\langle \cdot \rangle$ is a space-time average. Once a statistically stationary state has been reached, the time-average of (6) is equal to (7). In the present work, the Nusselt number was calculated using (6) and (7) with identical results.

2.2. Variational Multiscale Formulation for Rayleigh-Bénard Convection

The variational statement of the equations governing Rayleigh-Bénard convection is: *Find* $\mathbf{U} \in \mathcal{V}$ s.t. $\forall \mathbf{W} \in \mathcal{V}$

$$\mathcal{A}(\mathbf{W}, \mathbf{U}) = (\mathbf{W}, \mathbf{F}) \quad (8)$$

where $\mathbf{U} = [\mathbf{u}, P, T]^T$ is a vector of solutions, $\mathbf{W} = [\mathbf{w}, q, s]^T$ is a vector of weighting functions, and $\mathbf{F} = [\mathbf{f}^V, 0, \mathbf{f}^T]^T$ is a vector of forcing functions. Note that in the current work this forcing is zero. As per usual convection, the notation (\cdot, \cdot) denotes

an L_2 inner product of two functions over the domain Ω . The semilinear form (8) is,

$$\mathcal{A}(\mathbf{W}, \mathbf{U}) = \mathcal{A}^V(\mathbf{W}, \mathbf{U}) + (q, \nabla \cdot \mathbf{u}) + \mathcal{A}^T(\mathbf{W}, \mathbf{U}) \quad (9)$$

where

$$\begin{aligned} \mathcal{A}^V(\mathbf{W}, \mathbf{U}) = & \left(\mathbf{w}, \rho_0 \frac{\partial \mathbf{u}}{\partial t} \right) - (\nabla \mathbf{w}, \rho_0 \mathbf{u} \otimes \mathbf{u}) - (\nabla \cdot \mathbf{w}, P) \\ & + (\nabla \mathbf{w}, \mu \nabla \mathbf{u}) - (\mathbf{w}, \alpha_V g (T - T_0) \hat{\mathbf{y}}) \end{aligned} \quad (10)$$

$$\begin{aligned} \mathcal{A}^T(\mathbf{W}, \mathbf{U}) = & \left(s, \rho_0 C_p \frac{\partial T}{\partial t} \right) - (\nabla s, \rho_0 C_p \mathbf{u} T) \\ & + (\nabla s, k \nabla T). \end{aligned} \quad (11)$$

No boundary terms appear in the variational formulation due to the periodic, Dirichlet, and homogeneous Neumann boundary conditions in the problems considered in this work.

We consider a finite element method in which the discretized solutions $\mathbf{U}^h \in \mathcal{V}^h \subset \mathcal{V}$ are linear combinations of bilinear quadrilateral or hexahedral basis functions. The straightforward discretization leading to the Galerkin statement: *Find* $\mathbf{U}^h \in \mathcal{V}^h$ s.t. $\forall \mathbf{W}^h \in \mathcal{V}^h$, $\mathcal{A}(\mathbf{W}^h, \mathbf{U}^h) = (\mathbf{W}^h, \mathbf{F})$ is not sufficient due to the instabilities inherent in the Galerkin method for highly convective flows. To overcome this limitation, we develop a mixed variational multiscale formulation for Rayleigh-Bénard convection. The VMS method induces a sum-decomposition of the solution field \mathbf{U} into resolved \mathbf{U}^h and unresolved \mathbf{U}' components so that $\mathbf{U} = \mathbf{U}^h + \mathbf{U}'$. The resulting VMS formulation for

our problem with linear finite elements is: *Find* $\mathbf{U}^h \in \mathcal{V}^h$ s.t. $\forall \mathbf{W}^h \in \mathcal{V}^h$

$$\begin{aligned} \mathcal{A}(\mathbf{W}^h, \mathbf{U}^h) - & \underbrace{(\nabla \mathbf{w}^h, \rho_0 \mathbf{u}^h \otimes \mathbf{u}')}_{\text{VMS cross stresses}} - \underbrace{(\nabla \mathbf{w}^h, \rho_0 \mathbf{u}' \otimes \mathbf{u}^h)}_{\text{SUPG}} \\ & - \underbrace{(\nabla \mathbf{w}^h, \rho_0 \mathbf{u}' \otimes \mathbf{u}')}_{\text{Reynolds stresses}} - (\nabla \cdot \mathbf{w}^h, P') - (\mathbf{w}^h, \alpha_V g T' \hat{\mathbf{y}}) \\ & - (\nabla q^h, \mathbf{u}') \\ & - \underbrace{(\nabla s^h, \rho_0 C_p \mathbf{u}^h T')}_{T \text{ SUPG}} - \underbrace{(\nabla s^h, \rho_0 C_p \mathbf{u}' T^h)}_{T \text{ VMS cross stresses}} \\ & - \underbrace{(\nabla s^h, \rho_0 C_p \mathbf{u}' T')}_{T \text{ Reynolds stresses}} \\ = & (\mathbf{W}^h, \mathbf{F}). \end{aligned} \quad (12)$$

The formulation in (12) neglects terms involving time derivatives of unresolved fields as well as inner products of gradients of resolved and unresolved fields. Although not pursued here, approaches exist to model the transient effects of the unresolved scales [30]. In residual-based VMS formulations, the unresolved fields are proportional to the residual of the partial differential equations (PDEs),

$$\mathbf{U}' \approx -\tau \mathcal{R}(\mathbf{U}^h) \quad (13)$$

where

$$\mathcal{R}(\mathbf{U}^h) = \begin{bmatrix} \rho_0 \frac{\partial \mathbf{u}^h}{\partial t} + \rho_0 \nabla \cdot (\mathbf{u}^h \otimes \mathbf{u}^h) + \nabla P^h - \mu \nabla^2 \mathbf{u}^h - \alpha_V g (T^h - T_0) \hat{\mathbf{y}} \\ \nabla \cdot \mathbf{u}^h \\ \rho_0 C_p \left(\frac{\partial T^h}{\partial t} + \nabla \cdot (\mathbf{u}^h T^h) \right) - k \nabla^2 T^h \end{bmatrix} \quad (14)$$

and τ is the stabilization matrix. We use a diagonal stabilization matrix $\tau = \text{diag}(\tau_{ii}^V, \tau^C, \tau^T)$ where

$$\tau_{ii}^V = \left[\left(\frac{2C_i^V \rho_0}{\Delta t} \right)^2 + \rho_0^2 \mathbf{u}^h \cdot \mathbf{G} \mathbf{u}^h + (C_1 \mu)^2 \|\mathbf{G}\|^2 + \rho_0^2 \alpha_V g \|T^h\| \|\mathbf{G}\|^{1/2} \right]^{-1/2}, \quad i = 1, \dots, n_{sd} \quad (15)$$

$$\tau^C = (C_i^V \text{trace}(\mathbf{G}) \tau^V)^{-1} \quad (16)$$

$$\tau^T = \left[\left(\frac{2C_i \rho_0 C_p}{\Delta t} \right)^2 + (\rho_0 C_p)^2 \mathbf{u}^h \cdot \mathbf{G} \mathbf{u}^h + (C_1 k)^2 \|\mathbf{G}\|^2 \right]^{-1/2}, \quad (17)$$

\mathbf{G} is the metric tensor, n_{sd} the number of spatial dimensions, Δt is the time-step, and $C_1 = C_i = 1$. The components of the metric tensor \mathbf{G} are given by,

$$G_{ij} = \frac{\partial \xi_k}{\partial x_i} \frac{\partial \xi_k}{\partial x_j} \quad (18)$$

where ξ are the coordinates in the parametric (finite element) space. The first-order approximation to the unresolved scales (13) has been shown to be insufficient to model correlations of unresolved scales (the Reynolds stresses, $\mathbf{u}' \otimes \mathbf{u}'$ and $\mathbf{u}' T'$) for highly turbulent flows [31]. We expect the Reynolds

stresses to play a role in high Ra Rayleigh-Bénard convection. One option to more accurately model the Reynolds stress terms is to work with higher-order methods [32, 24]. An alternative approach is to introduce a mixed model wherein the Reynolds stresses are modeled by a classical eddy viscosity model (EVM) [33, 34, 26]. The mixed-model for Rayleigh-Bénard convection is: $Find \mathbf{U}^h \in \mathcal{V}^h$ s.t. $\forall \mathbf{W}^h \in \mathcal{V}^h$

$$\begin{aligned} \mathcal{A}(\mathbf{W}^h, \mathbf{U}^h) &- C_{\text{VMS}}^V (\nabla \mathbf{w}^h, \rho_0 \mathbf{u}^h \otimes \mathbf{u}') - C_{\text{SUPG}}^V (\nabla \mathbf{w}^h, \rho_0 \mathbf{u}' \otimes \mathbf{u}^h) \\ &- C_P^V (\nabla \cdot \mathbf{w}^h, P') + C_B^V (\mathbf{w}^h, \alpha_V g T' \hat{\mathbf{y}}) - C_{\text{PSPG}}^V (\nabla q^h, \mathbf{u}') \\ &- C_{\text{VMS}}^T (\nabla s^h, \mathbf{u}^h T') - C_{\text{SUPG}}^T (\nabla s^h, \mathbf{u}' T^h) - \\ &+ C_{\text{EVM}}^V (\nabla \mathbf{w}^h, \nu_T \nabla^s \mathbf{u}^h) + C_{\text{EVM}}^T (\nabla s^h, \rho_0 C_p \kappa_T \nabla T^h) \\ &= (\mathbf{W}^h, \mathbf{F}) \end{aligned} \quad (19)$$

where $\nabla^s \mathbf{u} = (\nabla \mathbf{u} + (\nabla \mathbf{u})^T) / 2$. In (19), the first term on the first line represents the Galerkin discretization, the second term represents a VMS cross-stress term, and the third term represents the SUPG stabilization. The first term on the second line is the pressure stabilization term, the second term represents temperature fluctuations in the buoyancy term, and the third term is used to overcome the inf-sup condition for finite element discretizations of the incompressible Navier-Stokes equations. The first term on the third line is an upwinding stabilization term for the temperature advection-diffusion equation and the second term is an additional cross-stress term from the VMS formulation. Finally, the fourth line includes the EVMs that are used to model the Reynolds stress terms. We have also included coefficients before each term which can be used to toggle various models on and off. The simulations in the current study are performed with two versions of (19). The first version is a straight VMS implementation neglecting the Reynolds stresses in addition to the other neglected terms mentioned above. The second version uses a modified VMS formulation and incorporates the Wall-Adapting Local Eddy-viscosity (WALE) model [35]. The WALE model possesses several desirable properties including that ν_T naturally approaches zero near the wall. In classical wall-bounded flows, the WALE model also recovers the correct asymptotic behavior of ν_T near the wall, $\nu_T \sim y^3$ for $y \rightarrow 0$. The VMS-WALE mixed model in the current work uses the SUPG stabilization terms as well as the VMS terms for the velocity-pressure saddle point system. In this way, the VMS-WALE model corresponds to a classical finite element WALE simulation with the necessary stabilization terms. Table 1 provides a summary of the toggling coefficients used in this study. As a final remark, we note that when using linear finite elements, the diffusive terms in the PDE residual are identically zero. In the Rayleigh-Bénard convection problem, these diffusive fluxes may play a key role and neglecting them in the residual may have a negative impact on the final solution [36]. We leave the development and implementation of such models for future work.

2.3. Numerical Methodology

All simulations were conducted using the Drekar finite element code [37, 38] using linear quadrilateral or hexahedral fi-

Coefficient	VMS Model	VMS-WALE
C_{VMS}^V	1	0
C_{SUPG}^V	1	1
C_P^V	1	1
C_B^V	1	0
C_{PSPG}^V	1	1
C_{VMS}^T	1	0
C_{EVM}^V	0	1
C_{EVM}^T	0	1

Table 1: Selected parameters in the mixed VMS-EVM model (19) for the two models used in the current study.

nite elements. The 2D simulations used an SDIRK22 (singly diagonally implicit Runge-Kutta 2nd order, 2 stage) time-integration method while the 3D simulations used a second order BDF method. The two-dimensional computations were run on up to 2000 cores while the three-dimensional simulations were run on up to 8000 cores. All simulations were performed on a capacity cluster with an Intel Haswell based CPU. The following section provides a broad overview of the time integration and solver formulations used to perform the simulations.

2.3.1. Fully-implicit Time Integration and Strongly-coupled Newton-Krylov-AMG Solver

Fully-implicit formulations, coupled with effective robust nonlinear iterative solution methods, have the potential to provide stable, higher-order time-integration of multiphysics systems when long dynamical time-scales are of interest. These methods can follow the desired dynamical time-scales as opposed to time-scales determined by either numerical stability or by temporal order-of-accuracy reduction [39, 40, 41, 42, 43, 37, 38]. For time-integration of the governing equations in (1) - (3), the L-stable SDIRK22 method is used [37, 38] as it provides a high-order time integration with damping of the highest unresolved wavenumbers [44].

A finite element discretization of the VMS equations (12) gives rise to a system of coupled, nonlinear, nonsymmetric algebraic equations, the numerical solution of which can be very challenging. These equations are linearized using an inexact form of Newton’s method. A formal block matrix representation of these discrete linearized equations is given by

$$\begin{bmatrix} \mathbf{D}_u & \mathbf{B}^T & \mathbf{Q} \\ \mathbf{B} & \mathbf{L}_P & \mathbf{0} \\ \mathbf{C} & \mathbf{0} & \mathbf{D}_T \end{bmatrix} \begin{bmatrix} \delta \hat{\mathbf{u}} \\ \delta \hat{\mathbf{P}} \\ \delta \hat{\mathbf{T}} \end{bmatrix} = - \begin{bmatrix} \mathbf{F}_u \\ \mathbf{F}_P \\ \mathbf{F}_T \end{bmatrix}.$$

where the block diagonal contribution of the stabilization procedure has been highlighted by a specific ordering. The block matrix, \mathbf{D}_u , corresponds to the discrete transient, convection, diffusion and stress terms acting on the unknowns $\delta \hat{\mathbf{u}}$; the matrix \mathbf{B}^T corresponds to the discrete gradient operator; \mathbf{B} , the divergence operator; the block matrix \mathbf{D}_T corresponds to the discrete transient, convection, diffusion operator acting on the temperature, and the matrix \mathbf{L}_P corresponds to the discrete “pres-

sure Laplacian". The matrix \mathbf{Q} corresponds to the coupling of velocity and the temperature field (buoyancy term), and the matrix \mathbf{C} the coupling of temperature gradient to the velocity field. The right hand side vectors contain the residuals for Newton's method. The existence of the nonzero matrix \mathbf{L}_p in the stabilized finite element discretization, is in contrast to Galerkin methods for incompressible flow using mixed interpolation that produce a zero block on the total mass continuity diagonal. The existence of this block matrix helps to enable the solution of the linear systems with a number of algebraic, domain decomposition (DD), and algebraic multilevel (AMG) type preconditioners/smoothers that rely on non-pivoting ILU type factorization, or in some cases methods such as Jacobi or Gauss-Seidel as sub-domain solvers [37, 38]. Although the above formal block matrix representation provides insight into the system, the actual linear algebra implementation in the application employs an ordering by finite element mesh node with each degree of freedom (dof) ordered consecutively. The Jacobian is evaluated analytically using automatic differentiation [45].

Fully-coupled Newton-Krylov techniques [46] where a Krylov solver is used to solve the linear system generated by a Newton's method are robust. However, efficient solution of the large sparse linear system that must be solved for each nonlinear iteration is challenging [47, 48]. The performance and scalability of the preconditioner is critical [47]. It is well known in the literature that Schwarz DD preconditioners do not scale due to lack of global coupling [49]. Multigrid methods are one of the most efficient techniques for solving large linear systems [50]. A Newton-Krylov preconditioned by AMG solution method has been described in our previous work in detail [48, 51, 37, 38, 52] and we will therefore only provide a very brief description here.

A Newton-Krylov (NK) method is an implementation of Newton's method in which a Krylov iterative solution technique is used to approximately solve the linear systems, $\mathbf{J}_k \mathbf{s}_{k+1} = -\mathbf{F}_k$, that are generated at each step of Newton's method. For efficiency, an inexact Newton method [53, 54, 55] is usually employed, whereby one approximately solves the linear systems generated in the Newton method by choosing a forcing term η_k and stopping the Krylov iteration when the inexact Newton condition, $\|\mathbf{F}_k + \mathbf{J}_k \mathbf{s}_{k+1}\| \leq \eta_{k+1} \|\mathbf{F}_k\|$ is satisfied. The particular Krylov method that is used in this study is a robust non-restarted GMRES method that is capable of iteratively converging to the solution of very large non-symmetric linear systems provided a sufficiently robust and scalable preconditioning method is available [48, 51, 37, 38, 52]. Two nonlinear convergence criteria are used to ensure that the numerical solution error is below discretization error. The first is a sufficient reduction in the relative nonlinear residual norm, $\|F_k\|/\|F_o\| < 10^{-2}$. In general, and specifically in the results presented in this paper, this requirement is easily satisfied. The second convergence criterion is based on a sufficient decrease of a weighted norm of the Newton update vector. This latter criterion requires that the correction, $\Delta\chi_i^k$, for any variable, χ_i , is small compared to its

magnitude, $|\chi_i^k|$, and is given by

$$\sqrt{\frac{1}{N_u} \sum_{i=1}^{N_u} \left[\frac{|\Delta\chi_i|}{\varepsilon_r |\chi_i| + \varepsilon_a} \right]^2} < 1,$$

where N_u is the total number of unknowns, ε_r is the relative error tolerance between the variable correction and its magnitude, and ε_a is the absolute error tolerance of the variable correction. Essentially ε_a sets the magnitude of components that are to be considered to be numerically zero. In the numerical results that are presented in this paper the relative-error, and absolute-error tolerance are set to 10^{-3} and 10^{-6} respectively for all of the test cases. In general, each linear system in Newton's method is solved to a moderate level of accuracy (e.g. $\eta = 10^{-3}$) since the outer nonlinear Newton iteration controls convergence at each time step.

A scalable preconditioner for the iterative linear solver is necessary to achieve solutions efficiently. For this reason, a fully-coupled algebraic multigrid method is employed [56]. In general AMG methods are significantly easier to implement and integrate with complex unstructured mesh discretizations than geometric multigrid methods [57, 58, 59]. Our fully-coupled AMG preconditioner employs a nonsmoothed aggregation approach with uncoupled aggregation. For systems of partial differential equations (PDEs), aggregation is performed on the graph where all the PDEs per mesh node are represented by a single vertex, as in our VMS discretization of the governing equations with each dof ordered at each finite element node consecutively. The discrete equations are projected to the coarser level employing a Galerkin projection with a triple matrix product, $A_{\ell+1} = R_\ell A_\ell P_\ell$, where R_ℓ restricts the residual from level ℓ to level $\ell+1$, A_ℓ is the discretization matrix on level ℓ and P_ℓ prolongates the correction from level $\ell+1$ to ℓ . We typically employ both pre- and post-smoothing on each level of the multigrid V-cycle except the coarsest level where a serial sparse direct solve is performed. In the computations carried out in this study the AMG preconditioner employs a DD-ILU(k) smoother with one level of overlap and a moderate level of fill-in (e.g. $k = 1$) A detailed discussion of the scalability of the solvers and comparisons of differing preconditioning techniques is out of scope of this study. However these fully-coupled Newton-Krylov-AMG solver have been studied extensively, with results demonstrating scaling on up to 1M+ cores for challenging resistive MHD type problems [38, 52].

3. Results

VMS-based large eddy simulations of Rayleigh-Bénard convection were run in two- and three-dimensional domains. In both cases, the no-slip boundary condition was used for the velocity field on all surfaces while the temperature field was prescribed at the top and bottom surfaces. Statistics such as the Nusselt number were obtained after the simulations reached a statistically steady state by averaging over a number of free-fall times, $t_f = H/U_f$ where the free-fall velocity is given by,

$$U_f = \sqrt{g\alpha_v \Delta T H}. \quad (20)$$

3.1. VMS Simulations of Two-dimensional Rayleigh-Bénard Convection

Two-dimensional simulations were run at $Pr = 1$. The aspect ratio for the two-dimensional problem was equal to 2 and periodic boundary conditions were used in the streamwise (x) direction. Two types of meshes were used for the 2D simulations. The first mesh used a uniform discretization in both coordinate directions. The second type of mesh was uniform in the x - direction but stretched in the y - direction. The stretching was accomplished using,

$$y_j^s = \frac{H}{2} \left(1 - \cos \left(\frac{(y_j - y_B)\pi}{H} \right) \right) + y_B, \quad j = 0, \dots, N_y \quad (21)$$

where $y_j = j\Delta y + y_B$, Δy is a uniform mesh spacing, N_y is the number of elements in the wall-normal direction, and y_B and y_T are the bottom and top coordinates of the plates, respectively. For all of the two-dimensional simulations, $y_T = 1$ and $y_B = -1$ leading to $H = 2$. We note that, especially for the high Ra cases, the simulations may be under-resolved in the boundary layer. This may have significant implications for the Nu results. Even so, the residual-based LES models do provide some measure of robustness and adaptivity in the near-wall region. For $Ra = 10^{13}$, we found $y^+ < 1$, which is an indication that the mesh is resolved. However, a more rigorous mesh convergence study should be performed. All statistics were measured after the simulations reached a statistically steady state. A representative temporal evolution of Nu is presented in Figure 1 for $Ra = 10^{13}$. The lightly-shaded region represents the transient portion and transition to a statistically steady state while the darkly-shaded region depicts the period within which statistics were collected. A representative snapshot of the temperature

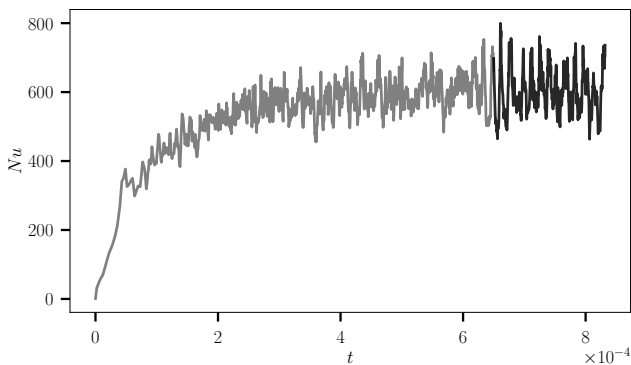


Figure 1: Nusselt evolution showing development to the statistically steady state. Statistics were collected in the statistically stationary region, indicated here by the darkly-shaded region.

field from the statistically steady portion of the simulation is presented in Figure 2. The visualization uses a Schlieren-type coloring to bring out the features of the flow. Table 2 presents a summary of the simulation parameters and results for the 2D VMS runs.

The $Nu - Ra$ scaling for the 2D VMS simulations is compared to recent 2D DNS results in Figure 3. The 2D VMS and DNS results are in excellent agreement up to $Ra \approx 10^{13}$ at

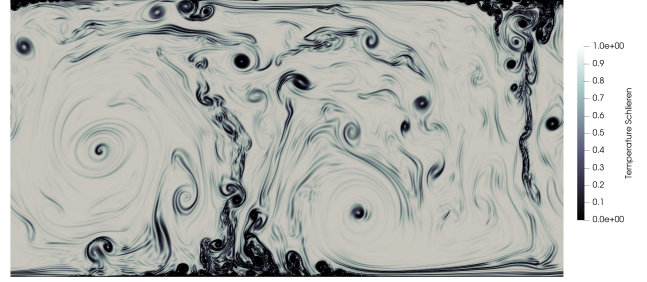


Figure 2: Temperature snapshot of the $Ra = 10^{13}$ simulation using a Schlieren-type visualization.

Ra	Nu	N_x	N_y	n_f	Mesh
10^6	8.21	128	128	2250	Uniform
10^7	13.4	256	256	3160	Non-uniform
10^8	24.9	512	256	170	Uniform
$2 \cdot 10^8$	28.3	512	256	664	Uniform
10^9	43.1	512	256	761	Non-uniform
10^{10}	89.8	512	256	1480	Non-uniform
10^{11}	175	512	256	644	Non-uniform
10^{12}	347	650	350	192	Non-uniform
10^{13}	601	750	500	144	Non-uniform
10^{14}	1172	750	500	139	Non-uniform

Table 2: Simulation parameters and results for the two-dimensional runs. N_x and N_y are the number of linear finite elements used for spatial discretization. n_f represents the number of free-fall times over which statistics were computed. The last column indicates if a uniform or stretched mesh was used in the wall-normal direction.

which point the DNS results indicate an increase in transport. Recent work [18, 19] has reported observations of a possible transition to the ultimate regime in direct numerical simulations of two-dimensional Rayleigh-Bénard convection. Although the present VMS results do not indicate such a transition, we emphasize that the VMS simulations may be under-resolved in the boundary layer. Additional research is needed to determine the effectiveness of the VMS simulations for an under-resolved boundary layer. In this particular study, the 2D VMS simulations show $Nu = 0.151Ra^{0.278}$ for $10^{10} \leq Ra \leq 10^{14}$.

3.2. VMS-WALE Model Simulations of Three-dimensional Rayleigh-Bénard Convection

The three-dimensional simulations were performed at $Pr = 7$ in a circular cylinder of aspect ratio 1/4. The height of the cylinder was $H = 100$ for each case. Homogeneous Neumann boundary conditions were used for the temperature on the surface of the cylinder. No-slip velocity boundary conditions were used on all surfaces of the cylinder. Most of the 3D simulations used the classical WALE model [35, 60] as an eddy viscosity model in the VMS formulation with a turbulent Prandtl number equal to unity. This corresponds to the WALE-VMS model in Table 1. Table 3 provides a summary of the simulation parameters and results for the three-dimensional simulations with the WALE-VMS model. The results from the WALE-VMS model were compared to SUPG and VMS results using a sequence of

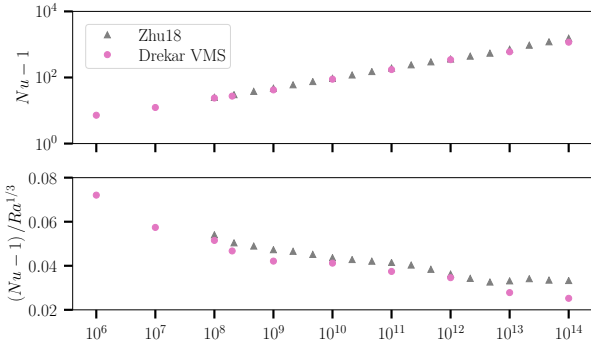


Figure 3: Top: Nusselt-Rayleigh scaling of the 2D simulations showing good agreement between the VMS and DNS results. Bottom: Nusselt-Rayleigh scaling plot compensated by the classical $Ra^{1/3}$ scaling. The VMS simulations show a scaling closer to $2/7$ than $1/3$ while the DNS results show a transition to the $1/3$ scaling.

Ra	Nu	N_y	$N_{r\theta}$	Mesh Elements	n_f
10^{10}	131.8	336	7344	2467584	106.4
10^{11}	267.6	256	4620	1182720	99.2
10^{12}	565.0	336	7344	2467584	442.8
10^{13}	1121.5	380	13500	5130000	90.4
10^{14}	2275.5	500	20800	10400000	37.78

Table 3: Simulation parameters and results for the three-dimensional runs. N_y and $N_{r\theta}$ represent the number of elements in the vertical direction and in the $r-\theta$ plane, respectively. n_f represents the number of free-fall times over which statistics were computed.

finer meshes at $Ra = 10^{10}$. Table 4 compares the Nusselt number between these three models at the finest mesh. At this mesh resolution, all three models are in good agreement. Figure 4 shows a snapshot of the temperature field at $Ra = 10^{10}$ taken at a plane in the boundary layer ($y = 0.001$) for the simulations in the cylinder. Similarly to the 2D runs, the $y+$ value was computed and determined to be less than 1 for most runs. Figure 5 presents temperature contours colored by vertical velocity at $Ra = 10^{10}$.

The Nusselt-Rayleigh scaling is presented in Figure 6. The results are presented over several decades of Ra for a number of studies, including the present results. The results from the VMS models compare favorably to direct numerical simulations as well as experiments and the classical $Nu \propto Ra^{1/3}$ scaling emerges over several decades in Ra . In particular, the VMS-WALE model shows a scaling of $Nu = 0.104Ra^{0.310}$ for $10^{10} \leq Ra \leq 10^{14}$, while very recent DNS results show $Nu = 0.0525Ra^{0.331}$ for $10^{10} \leq Ra \leq 10^{15}$ [17].

Ra	Mesh Elements	VMS	VMS-WALE	SUPG
10^{10}	2,467,584	131.1	131.8	131.7

Table 4: Comparison of Nu at $Ra = 10^{10}$ between simulations in an aspect ratio 1/4 cylinder using the VMS, VMS-WALE, and SUPG models.

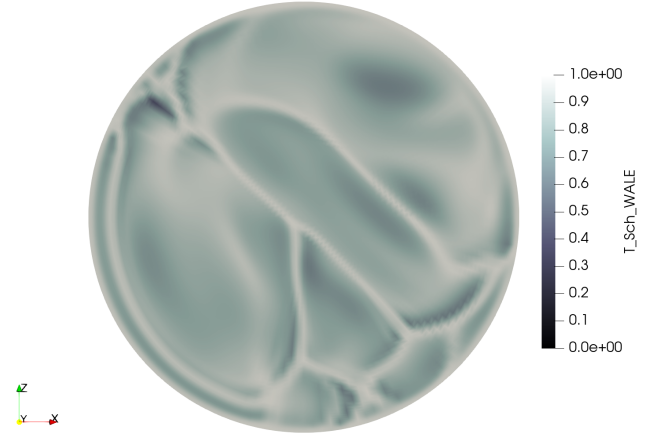


Figure 4: Temperature snapshot in a plane within the boundary layer at $y = 0.001$ using a Schlieren visualization from the VMS-WALE simulation in the cylinder geometry.

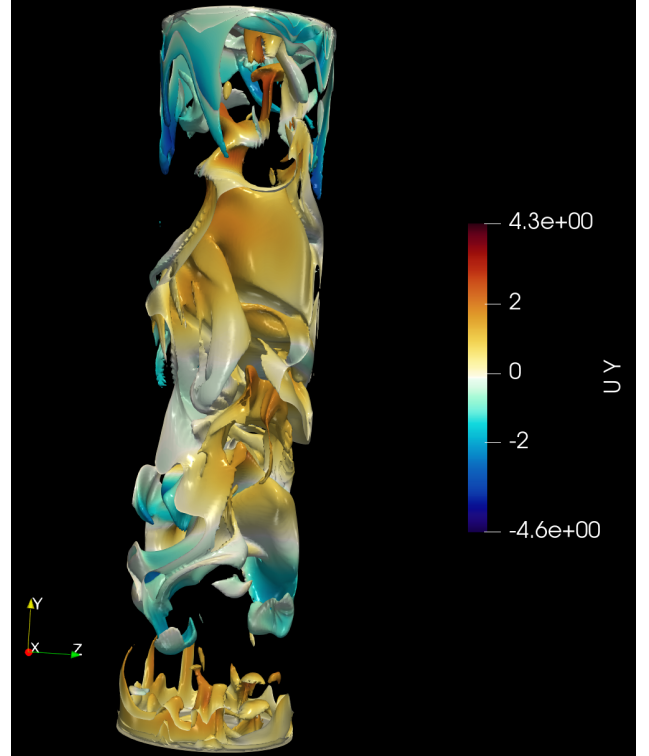


Figure 5: Temperature contours colored by vertical velocity at $Ra = 10^{10}$.

4. Conclusions

A residual-based VMS formulation was derived for Rayleigh-Bénard convection and augmented with eddy viscosity models to account for the Reynolds stresses. This new mixed model was implemented in the finite element code Drekar. In the current work, the WALE model was used for the eddy viscosity model. A number of two and three dimensional simulations were performed to compute the heat transport scaling in each system up to $Ra = 10^{14}$. The new VMS simulations are in good agreement with previous direct numerical simulations of two- and three- dimensional Rayleigh-Bénard convection re-

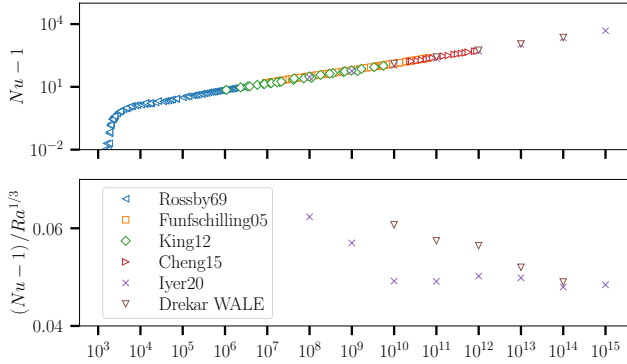


Figure 6: Nusselt-Rayleigh scaling for a variety of experimental and numerical studies: [61]—blue, right-pointing triangles; [62, 63]—orange squares; [64]—green diamonds; [65]—red, right pointing triangles; [17]—purple exes; this work—brown, downward pointing triangles.

sults. When compared to recent 2D DNS simulations, the VMS simulations begin to show a difference in $Nu - Ra$ scaling at around $Ra = 10^{13}$. Before claiming this as evidence for the absence of a transition to the ultimate regime, we suggest several avenues for additional research regarding the VMS models.

Resolution of the boundary layer in Rayleigh-Bénard convection is critical [66]. Residual-based VMS formulations have an ability to automatically adapt to regions of the flow that are under-resolved, but this may not be sufficient to capture the underlying heat release from the boundary layer. Moreover, when using linear finite elements, the viscous terms in the residual vanish identically. The impact of this incomplete residual on the $Nu - Ra$ scaling should be assessed. Previous work has introduced techniques for reconstructing the diffusive flux for linear finite elements [36]. We have implemented this diffusive flux reconstruction into the Drekar code and are currently testing its impact on Rayleigh-Bénard convection. In addition to the diffusive flux reconstruction, a more thorough mesh convergence study should be performed along with a rigorous assessment of the near-wall behavior of the models. Comparisons to simulations that use higher-order elements would also provide a useful perspective.

Beyond Rayleigh-Bénard convection, we will implement and use VMS models on rotating Rayleigh-Bénard convection. Early results from Drekar compare favorably with experiments in this regime. Additional future work will include magneto-convection with applications to geophysical and astrophysical problems.

Acknowledgments

The authors would like to thank Professor Jon A. Aurnou (UCLA) for sharing data from their experimental system. The work of John N. Shadid, Roger P. Pawlowski, Thomas Smith, and Sidafa Conde was partially supported by the U.S. Department of Energy, Office of Science, Office of Advanced Scientific Computing Research. Sandia National Laboratories is a multi-mission laboratory managed and operated by National Technology and Engineering Solutions of Sandia, LLC, a wholly owned subsidiary of Honeywell International, Inc.,

for the U.S. Department of Energy’s National Nuclear Security Administration under contract DE-NA0003525. This paper describes objective technical results and analysis. Any subjective views or opinions that might be expressed in the paper do not necessarily represent the views of the U.S. Department of Energy or the United States Government.

References

- [1] P. G. Drazin, W. H. Reid, Hydrodynamic stability, Cambridge university press, 2004.
- [2] S. Chandrasekhar, Hydrodynamic and hydromagnetic stability, Courier Corporation, 2013.
- [3] L. Rayleigh, LIX. on convection currents in a horizontal layer of fluid, when the higher temperature is on the under side, The London, Edinburgh, and Dublin Philosophical Magazine and Journal of Science 32 (192) (1916) 529–546.
- [4] E. Bodenschatz, W. Pesch, G. Ahlers, Recent developments in Rayleigh-Bénard convection, Annual review of fluid mechanics 32 (1) (2000) 709–778.
- [5] G. Ahlers, S. Grossmann, D. Lohse, Heat transfer and large scale dynamics in turbulent Rayleigh-Bénard convection, Reviews of modern physics 81 (2) (2009) 503.
- [6] W. V. Malkus, The heat transport and spectrum of thermal turbulence, Proceedings of the Royal Society of London. Series A. Mathematical and Physical Sciences 225 (1161) (1954) 196–212.
- [7] L. N. Howard, Convection at high Rayleigh number, in: Applied Mechanics, Springer, 1966, pp. 1109–1115.
- [8] C. R. Doering, P. Constantin, Variational bounds on energy dissipation in incompressible flows. III. convection, Physical Review E 53 (6) (1996) 5957.
- [9] Z. Ding, R. R. Kerswell, Exhausting the background approach for bounding the heat transport in Rayleigh-Bénard convection, arXiv preprint arXiv:1906.03376.
- [10] R. H. Kraichnan, Turbulent thermal convection at arbitrary Prandtl number, The Physics of Fluids 5 (11) (1962) 1374–1389.
- [11] S. Grossmann, D. Lohse, Scaling in thermal convection: a unifying theory, Journal of Fluid Mechanics 407 (2000) 27–56.
- [12] X. He, D. Funfschilling, H. Nobach, E. Bodenschatz, G. Ahlers, Transition to the ultimate state of turbulent Rayleigh-Bénard convection, Physical review letters 108 (2) (2012) 024502.
- [13] V. Bouillaut, S. Lepot, S. Aumaître, B. Gallet, Transition to the ultimate regime in a radiatively driven convection experiment, Journal of Fluid Mechanics 861.
- [14] J. Niemela, L. Skrbek, K. Sreenivasan, R. Donnelly, Turbulent convection at very high Rayleigh numbers, Nature 404 (6780) (2000) 837–840.
- [15] C. R. Doering, Thermal forcing and ‘classical’ and ‘ultimate’ regimes of Rayleigh-Bénard convection, Journal of Fluid Mechanics 868 (2019) 1–4.
- [16] R. J. Stevens, D. Lohse, R. Verzicco, Prandtl and Rayleigh number dependence of heat transport in high Rayleigh number thermal convection, Journal of Fluid Mechanics 688 (2011) 31–43.
- [17] K. P. Iyer, J. D. Scheel, J. Schumacher, K. R. Sreenivasan, Classical 1/3 scaling of convection holds up to $Ra = 10^{15}$, Proceedings of the National Academy of Sciences.
- [18] X. Zhu, V. Mathai, R. J. Stevens, R. Verzicco, D. Lohse, Transition to the ultimate regime in two-dimensional Rayleigh-Bénard convection, Physical Review Letters 120 (14) (2018) 144502.
- [19] X. Zhu, V. Mathai, R. J. Stevens, R. Verzicco, D. Lohse, Absence of evidence for the ultimate regime in two-dimensional Rayleigh-Bénard convection reply, Physical review letters 123 (2019) 259402.
- [20] A. N. Brooks, T. J. Hughes, Streamline upwind/petrov-galerkin formulations for convection dominated flows with particular emphasis on the incompressible navier-stokes equations, Computer Methods in Applied Mechanics and Engineering 32 (1-3) (1982) 199–259.
- [21] L. P. Franca, G. Hauke, A. Masud, Stabilized finite element methods, International Center for Numerical Methods in Engineering (CIMNE), Barcelona, Spain, 2004.
- [22] T. J. Hughes, Multiscale phenomena: Green’s functions, the dirichlet-to-neumann formulation, subgrid scale models, bubbles and the origins of

- stabilized methods, *Computer methods in applied mechanics and engineering* 127 (1-4) (1995) 387–401.
- [23] A. Masud, R. Khurram, A multiscale finite element method for the incompressible Navier-Stokes equations, *Computer Methods in Applied Mechanics and Engineering* 195 (13-16) (2006) 1750–1777.
- [24] Y. Bazilevs, V. Calo, J. Cottrell, T. Hughes, A. Reali, G. Scovazzi, Variational multiscale residual-based turbulence modeling for large eddy simulation of incompressible flows, *Computer Methods in Applied Mechanics and Engineering* 197 (1-4) (2007) 173–201.
- [25] J. Liu, A. Oberai, The residual-based variational multiscale formulation for the large eddy simulation of compressible flows, *Computer Methods in Applied Mechanics and Engineering* 245 (2012) 176–193.
- [26] D. Sondak, J. N. Shadid, A. A. Oberai, R. P. Pawlowski, E. C. Cyr, T. M. Smith, A new class of finite element variational multiscale turbulence models for incompressible magnetohydrodynamics, *Journal of Computational Physics* 295 (2015) 596–616.
- [27] R. Codina, On stabilized finite element methods for linear systems of convection–diffusion–reaction equations, *Computer Methods in Applied Mechanics and Engineering* 188 (1-3) (2000) 61–82.
- [28] R. Codina, S. Badia, J. Baiges, J. Principe, Variational multiscale methods in computational fluid dynamics, *Encyclopedia of Computational Mechanics Second Edition* (2018) 1–28.
- [29] S. Xu, B. Gao, M.-C. Hsu, B. Ganapathysubramanian, A residual-based variational multiscale method with weak imposition of boundary conditions for buoyancy-driven flows, *Computer Methods in Applied Mechanics and Engineering* 352 (2019) 345–368.
- [30] R. Codina, Stabilized finite element approximation of transient incompressible flows using orthogonal subscales, *Computer methods in applied mechanics and engineering* 191 (39-40) (2002) 4295–4321.
- [31] Z. Wang, A. Oberai, Spectral analysis of the dissipation of the residual-based variational multiscale method, *Computer Methods in Applied Mechanics and Engineering* 199 (13-16) (2010) 810–818.
- [32] T. J. Hughes, J. A. Cottrell, Y. Bazilevs, Isogeometric analysis: CAD, finite elements, NURBS, exact geometry and mesh refinement, *Computer methods in applied mechanics and engineering* 194 (39-41) (2005) 4135–4195.
- [33] Z. Wang, A. A. Oberai, A mixed large eddy simulation model based on the residual-based variational multiscale formulation, *Physics of Fluids* 22 (7) (2010) 075107.
- [34] A. A. Oberai, J. Liu, D. Sondak, T. Hughes, A residual based eddy viscosity model for the large eddy simulation of turbulent flows, *Computer Methods in Applied Mechanics and Engineering* 282 (2014) 54–70.
- [35] F. Nicoud, F. Ducros, Subgrid-scale stress modelling based on the square of the velocity gradient tensor, *Flow, Turbulence and Combustion* 62 (3) (1999) 183–200.
- [36] K. E. Jansen, S. S. Collis, C. Whiting, F. Shaki, A better consistency for low-order stabilized finite element methods, *Computer methods in applied mechanics and engineering* 174 (1-2) (1999) 153–170.
- [37] J. N. Shadid, R. P. Pawlowski, J. W. Banks, L. Chacón, P. T. Lin, R. S. Tuminaro, Towards a scalable fully-implicit fully-coupled resistive MHD formulation with stabilized FE methods, *J. Comput. Phys.* 229 (20) (2010) 7649–7671.
- [38] J. N. Shadid, R. P. Pawlowski, E. C. Cyr, R. S. Tuminaro, L. Chacon, P. D. Weber, Scalable Implicit Incompressible Resistive MHD with Stabilized FE and Fully-coupled Newton-Krylov-AMG, *Comput. Methods Appl. Mech. Engrg.* 304 (2016) 1–25.
- [39] C. C. Ober, J. N. Shadid, Studies on the accuracy of time-integration schemes for the radiation-diffusion equations, *J. Comp. Phys.* 195 (2) (2004) 743–772.
- [40] D. L. Ropp, J. N. Shadid, C. C. Ober, Studies of the accuracy of time integration methods for reaction-diffusion equations, *J. Comp. Phys.* 194 (2) (2004) 544–574.
- [41] D. Ropp, J. Shadid, Stability of operator splitting methods for systems with indefinite operators: reaction-diffusion systems, *J. Comp. Phys.* 203 (2005) 449–466.
- [42] D. A. Knoll, V. A. Mousseau, L. Chacón, J. Reisner, Jacobian-free Newton-Krylov methods for the accurate time integration of stiff wave systems, *SIAM J. Sci. Comput.* 25 (1) (2005) 213–230.
- [43] D. L. Ropp, J. N. Shadid, Stability of operator splitting methods for systems with indefinite operators: Advection-diffusion-reaction systems, *J. Comp. Phys.* 228 (2009) 3508–3516.
- [44] U. M. Ascher, L. R. Petzold, *Computer Methods for Ordinary Differential Equations and Differential-Algebraic Equations*, SIAM, 1998.
- [45] E. Phipps, R. Pawlowski, Efficient expression templates for operator overloading-based automatic differentiation, in: S. Forth, P. Hovland, E. Phipps, J. Utke, A. Walther (Eds.), *Recent Advances in Algorithmic Differentiation*, Vol. 87 of *Lecture Notes in Computational Science and Engineering*, Springer, Berlin, Heidelberg, 2012.
- [46] P. N. Brown, Y. Saad, Hybrid Krylov methods for nonlinear systems of equations, *SIAM J. Sci. Stat. Comput.* 11 (1990) 450–481.
- [47] D. A. Knoll, D. E. Keyes, Jacobian-free Newton–Krylov methods: a survey of approaches and applications, *J. Comput. Phys.* 193 (2004) 357–397.
- [48] P. T. Lin, M. Sala, J. N. Shadid, R. S. Tuminaro, Performance of fully-coupled algebraic multilevel domain decomposition preconditioners for incompressible flow and transport, *Int. J. Num. Meth. Eng.* 67 (9) (2006) 208–225.
- [49] B. Smith, P. Bjorstad, W. Gropp, *Domain Decomposition: Parallel Multi-level Methods for Elliptic Partial Differential Equations*, Cambridge University Press, 1996.
- [50] U. Trottenberg, C. Oosterlee, A. Schüller, *Multigrid*, Academic Press, London, 2001.
- [51] P. T. Lin, J. N. Shadid, M. Sala, R. S. Tuminaro, G. L. Hennigan, R. J. Hoekstra, Performance of a parallel algebraic multilevel preconditioner for stabilized finite element semiconductor device modeling, *Journal Computational Physics* 228 (2009) 6250–6267.
- [52] P. T. Lin, J. N. Shadid, J. J. Hu, R. P. Pawlowski, E. C. Cyr, Performance of fully-coupled algebraic multigrid preconditioners for large-scale VMS resistive MHD, *J. Comp. and Applied Math* 344 (2018) 782–793.
- [53] J. E. Dennis, Jr., R. B. Schnabel, *Numerical Methods for Unconstrained Optimization and Nonlinear Equations*, Series in Automatic Computation, Prentice-Hall, Englewood Cliffs, NJ, 1983.
- [54] S. C. Eisenstat, H. F. Walker, Choosing the forcing terms in an inexact Newton method, *SIAM J. Sci. Comput.* 17 (1996) 16–32.
- [55] J. N. Shadid, A fully-coupled Newton-Krylov solution method for parallel unstructured finite element fluid flow, heat and mass transfer simulations, *Int. J. Comput. Fluid Dynamics* 3-4 (1999) 199–211.
- [56] M. Gee, C. Siefert, J. Hu, R. Tuminaro, M. Sala, *ML 5.0 smoothed aggregation user’s guide*, Tech. Rep. SAND2006-2649, Sandia National Laboratories, Albuquerque NM, 87185 (2006).
- [57] R. Tuminaro, C. Tong, J. Shadid, K.D.Devine, D. Day, On a multilevel preconditioning module for unstructured mesh Krylov solvers: two-level schwarz, *Comm. Num. Method. Eng.* 18 (2002) 383–389.
- [58] J. Shadid, R. Tuminaro, K. Devine, G. Henningan, P. Lin, Performance of fully-coupled domain decomposition preconditioners for finite element transport/reaction simulations, *J. Comput. Phys.* 205 (1) (2005) 24–47.
- [59] J. N. Shadid, A. G. Salinger, R. P. Pawlowski, P. T. Lin, G. L. Hennigan, R. S. Tuminaro, R. B. Lehoucq, Stabilized FE computational analysis of nonlinear steady state transport/reaction systems, *Comp. Meth. Applied Mech. Eng.* 195 (2006) 1846–1871.
- [60] T. M. Smith, J. N. Shadid, R. P. Pawlowski, E. C. Cyr, P. D. Weber, Reactor core sub-assembly simulations using a stabilized finite element method, in: *NURETH-14-500, The 14th International Topical Meeting on Nuclear Reactor Thermalhydraulics, NURETH-14*, Toronto, Ontario, Canada, 2011.
- [61] H. Rossby, A study of Bénard convection with and without rotation, *Journal of Fluid Mechanics* 36 (2) (1969) 309–335.
- [62] D. Funfschilling, E. Brown, A. Nikolaenko, G. Ahlers, Heat transport by turbulent Rayleigh-Bénard convection in cylindrical samples with aspect ratio one and larger, *Journal of Fluid Mechanics* 536 (2005) 145–154.
- [63] A. Nikolaenko, E. Brown, D. Funfschilling, G. Ahlers, Heat transport by turbulent Rayleigh-Bénard convection in cylindrical cells with aspect ratio one and less, *Journal of Fluid Mechanics* 523 (2005) 251–260.
- [64] E. M. King, S. Stellmach, J. M. Aurnou, Heat transfer by rapidly rotating Rayleigh-Bénard convection, *Journal of Fluid Mechanics* 691 (2012) 568–582.
- [65] J. S. Cheng, S. Stellmach, A. Ribeiro, A. Grannan, E. M. King, J. M. Aurnou, Laboratory-numerical models of rapidly rotating convection in planetary cores, *Geophysical Journal International* 201 (1) (2015) 1–17.
- [66] G. Grötzbach, Spatial resolution requirements for direct numerical simulation of the Rayleigh-Bénard convection, *Journal of computational physics* 49 (2) (1983) 241–264.